International Journal of Heat and Mass Transfer 51 (2008) 6235–6242

Contents lists available at ScienceDirect

International Journal of Heat and Mass Transfer

journal homepage: www.elsevier.com/locate/ijhmt

Flow boiling of R134a and ammonia in a plate heat exchanger

E. Djordjevic [a], S. Kabelac [b,*]

[a] Faculty of Technology and Metallurgy, University of Belgrade, Karnegijeva 4, 11120 Belgrade, Serbia
[b] Institute for Thermodynamics, Helmut Schmidt University of the Federal Armed Forces, D-22039 Hamburg, Germany

ARTICLE INFO

Article history:
Received 29 March 2007
Received in revised form 25 November 2007
Available online 14 July 2008

Keywords:
Evaporation
Plate heat exchanger
Heat transfer coefficient
R134a
Ammonia

ABSTRACT

This paper presents experimental results on evaporation heat transfer for flow boiling of ammonia and of R134a in a chevron-pattern corrugated plate heat exchanger (PHE). The measurements enable the evaluation of a quasi-local heat transfer coefficient along the plate, which in turn allows discussing the two-phase distribution and the heat transfer mechanism during evaporation in a plate channel. The saturation temperature varied between $268\ \mathrm{K} < T^s_{\mathrm{NH3}} < 283\ \mathrm{K}$ ($3.55\ \mathrm{bar} < p^s_R < 5.73\ \mathrm{bar}$) for ammonia and $265\ \mathrm{K} < T^s_{\mathrm{R134a}} < 283\ \mathrm{K}$ ($2.157\ \mathrm{bar} < p^s_R < 4.14\ \mathrm{bar}$) for R134a. The heat transfer coefficient is discussed in relation to the vapor quality, mass flux, heat flux and the type of refrigerant. The secondary fluid is a water/ethylene glycol mixture flowing in counter flow or parallel flow arrangement within the PHE. It is shown that the parallel flow case yields better overall performance than the counterflow case, and that plates with low chevron angle corrugations increase the evaporation heat transfer. Comparison with the limited data available from the literature shows good agreement. The Danilova equation and the Steiner boiling correlation are adapted to PHEs and show the need for further theoretical development.

1. Introduction

Plate heat exchangers (PHE) are becoming common components in refrigeration and heat pump cycles, when a liquid is the heat donating fluid in the evaporator or the heat absorbing fluid in the condenser. Unfortunately, a physically based design algorithm for PHE evaporators or condensers is still missing, thus the design of these components is based on empirical correlations and on individual knowledge of PHE manufacturers, which often is proprietary. To establish useful correlations that are capable to predict the thermal-hydraulic behavior of PHE, a lot of experimental data for various operating conditions has to be gathered. Only then the data collection will allow for the development and validation of useful correlations for different fluids, different plate designs and different flow conditions. This has been demonstrated successfully e.g. by Steiner and Taborek, who derived their well-known correlation for evaporation heat transfer in tubes from a data base with more than 60.000 data points [1].

Already back in 1981, Danilova et al. have published some data on the evaporation of R12, R22, R113 and ammonia in PHEs and in plate-fin heat exchangers [2]. Their simple but interesting correlation will be further reviewed in Section 4. Within the last 10 years five groups have published experimental data on the evaporative heat transfer in PHEs. Yan and Lin as well as Hsieh and Lin [3,4] have published data on the evaporation of R134a ($298\ \mathrm{K} < T^s_R < 304\ \mathrm{K}; 6.75\ \mathrm{bar} < p^s_R < 8\ \mathrm{bar}$) and R410A ($283\ \mathrm{K} < T^s_R < 288\ \mathrm{K}; 10.8\ \mathrm{bar} < p^s_R < 12.5\ \mathrm{bar}$). They show a quasi-local heat transfer coefficient for a chevron type plate with a 60° chevron angle as a function of vapor quality, mass flux and heat flux. They used a preheater to adjust different vapor qualities at the inlet of the PHE, so that the vapor quality of the refrigerant changes only by about 10% inside the PHE. Thus, the average heat transfer coefficient extracted from these measurements may be considered to be quasi-local compared to a channel in which complete evaporation takes place; their data will be used for comparison in Section 4. Wellsandt [5] studied evaporation of R22 ($260\ \mathrm{K} < T^s_R < 280\ \mathrm{K}; 3.17\ \mathrm{bar} < p^s_R < 6.19\ \mathrm{bar}$) and R134a ($260\ \mathrm{K} < T^s_R < 280\ \mathrm{K}; 1.77\ \mathrm{bar} < p^s_R < 3.73\ \mathrm{bar}$) in a large plate-type evaporator of a heat pump. The plates were 3000 mm high and were attached to each other by 1300 welding points, resulting in 13 cross-connected vertical flow channels along the plate. Local temperature measurements along the plate allowed for temperature profiles but no local heat transfer coefficients as a function of vapor quality were given. Recently, Longo and Gasparella [6] published data on experimental overall heat transfer coefficients and pressure drop during R134a evaporation inside a small brazed PHE for saturation temperatures between 283 K and 303 K ($4.1\ \mathrm{bar} < p^s_R < 7.67\ \mathrm{bar}$). They have also studied the possible enhancement in heat transfer when corrugated plates are given a gross-grooved surface [7]. Sterner and Sunden have reported on measurements on the evaporation of ammonia ($270\ \mathrm{K} < T^s_R < 280\ \mathrm{K}; 3.81\ \mathrm{bar} < p^s_R < 5.51\ \mathrm{bar}$)

* Corresponding author. Tel.: +49 40 6541 2735; fax: +49 40 6541 2005.
E-mail address: kabelac@hsu-hh.de (S. Kabelac).

0017-9310/$ - see front matter © 2008 Elsevier Ltd. All rights reserved.
doi:10.1016/j.ijheatmasstransfer.2008.01.042

Nomenclature

A_i	heat transferring area of the control volume i (m^2)
a	wave amplitude of the chevron plate (m)
c_p	specific heat capacity (J/kg K)
d_h	hydraulic diameter in the Danilova correlation, $d_h = 4 \cdot a$
d_h^*	hydraulic diameter in the Martin correlation, $d_h^* = 4 \cdot a/\Phi$
g	acceleration of gravity (m/s^2)
h_H	local heat transfer coefficient on the heating fluid side (W/m^2 K)
h_R	local heat transfer coefficient on the refrigerant side (W/m^2 K)
$\dot{m}_H$	mass flux of the heating fluid within one plate channel (kg/m^2s)
$\dot{m}_R$	mass flux of the refrigerant within one plate channel (kg/m^2s)
$\dot{M}_H$	mass flow of the heating fluid (kg/s)
$\dot{M}_R$	mass flow of the refrigerant (kg/s)
p_R^s	saturation pressure of the refrigerant (bar)
$\dot{Q}$	heat flow through one plate (W)
$\dot{q}$	heat flux (W/m^2)
T_H	temperature of the heating fluid (°C)
T_R^s	saturation temperature of the refrigerant (°C)
$T_{w,H}$	wall surface temperature from the heating fluid side (°C)
$T_{w,R}$	wall surface temperature from the refrigerant side (°C)
U	overall heat transfer coefficient for the plate (W/m^2 K)
$\dot{x}$	vapor quality

Greek symbols

Δh_v	enthalpy of vaporization for the refrigerant (J/kg)
Δx_i	vapor production within control volume i (kg/kg)
δ_{pl}	plate thickness (m)
λ_{pl}	thermal conductivity of the plate material (W/m K)
Λ_{pl}	wave length of the chevron plate (m)
φ	chevron angle (°)
σ	surface tension (N/m)
η	dynamic viscosity (Pa s)
Φ	plate area extension factor [4]

Subscripts

i	number of segments, segment outlet value
$\bar{i}$	mean value for the segment
R	refrigerant value
H	heating fluid value
pl	plate

in semi-welded PHE and in nickel-brazed PHE [8]. They stated that an integrated inlet flow distributor gives a better performance in the case of having the expansion valve right in front of the evaporator (direct expansion operation mode). Experiments on the evaporative heat transfer and pressure drop in small brazed PHEs are reported by Han et al. [9]. Data for R410A in the range 278 K < T_s < 288 K (9.3 bar < p_s < 12.5 bar) as well as for R134a in the range 278 K < T_s < 288 K (5.8 bar < p_s < 7.86 bar) at different chevron angles, different mass flow rates and heat fluxes were obtained. It was found that the heat transfer coefficients of R410A are larger than those of R22 at comparable conditions.

All of these groups also give simple correlations fitted to their own data only, so these equations will not have much predictive capability. From these groups, Wellsandt [5] as well as Longo and Gasparella [6] have measured local temperatures inside the PHE along a plate. These data will contribute to the database to be set up, but it already becomes evident that basic questions about the relevant boiling mechanisms are still unresolved. While Thonon et al. conclude that the relevant evaporation mechanism is the convective boiling regime [10], Danilova et al. claims that only nucleate boiling should be considered in PHEs [2]. Our results indicate a nucleate boiling regime for higher heat fluxes. Sterner and Sunden [8] speculate that the relevant boiling mechanism changes from convective to nucleate dominated boiling at a certain critical channel dimension, which may depend on pressure and fluid properties. The abundant results known for boiling mechanisms in plain tubes with technical diameters cannot be simply transferred to compact plate type heat exchangers [12]. Even though the distribution of vapor quality along a plate is not well known, the annular flow regime seems to prevail more than in tubes due to a larger surface-to-volume ratio and surface tension influence. The conclusion by Yan and Lin [3], who state that the evaporation heat transfer coefficient in a PHE is higher than in "corresponding" tubes, is not supported by our results.

The aim of this work is to report on experimental quasi-local heat transfer coefficients as a function of vapor quality for different mass and heat fluxes. Two different plate geometries have been studied, counterflow as well as parallel flow situations were analysed. The quasi-local values will help to understand the temperature and vapor distribution along a plate during evaporation and help to resolve some of the questions named above. In the next section the experimental setup will be outlined, followed by a section explaining the data reduction. Results for heat transfer coefficients for R134a and ammonia are presented in Section 4.

2. Experimental setup

The experimental refrigeration system encloses two fluid loops that exchange heat as the primary fluid is evaporated and subsequently condensed in two PHEs with a secondary fluid acting as a heat carrier between the condenser and the evaporator; the setup is depicted in Fig. 1. The special feature of our experimental setup is the measurement of temperature profiles along a plate inside the PHE evaporator. With K-type thermocouples inserted through the gasket between two plates, nine fluid temperatures within one channel of the heating fluid (water/ethylene glycol) and seven wall temperatures on the plate surface facing the heating fluid were measured. Refrigerant temperatures were measured at the entrance and the exit of the PHE only. The locations of the thermocouples are shown in Fig. 2 for a high pressure drop plate designated type A with a chevron angle of $\varphi_A = 63°$. The temperature readings allow for local energy balances of volume segments along the plate, which finally result in quasi-local heat transfer coefficients as a function of vapor quality on the refrigerant side of the PHE. The evaluation scheme is described in the next section.

The plates of the commercial plate and frame heat exchanger used in the experiments are NT type stainless steel plates made by GEA Ecoflex GmbH, Germany. The major dimensions of a plate are given in Table 1. When using ammonia as a refrigerant, we also used a second type of plate with identical dimensions as given in Table 1 except for a chevron angle of $\varphi_B = 27°$, designated type B plates (low pressure drop plates). The evaporator PHE had 10 plates, forming four channels for the refrigerant and five channels for the heating fluid, an aqueous solution of 35% ethylene glycol. The wall temperature thermocouples are fixed onto the plates via

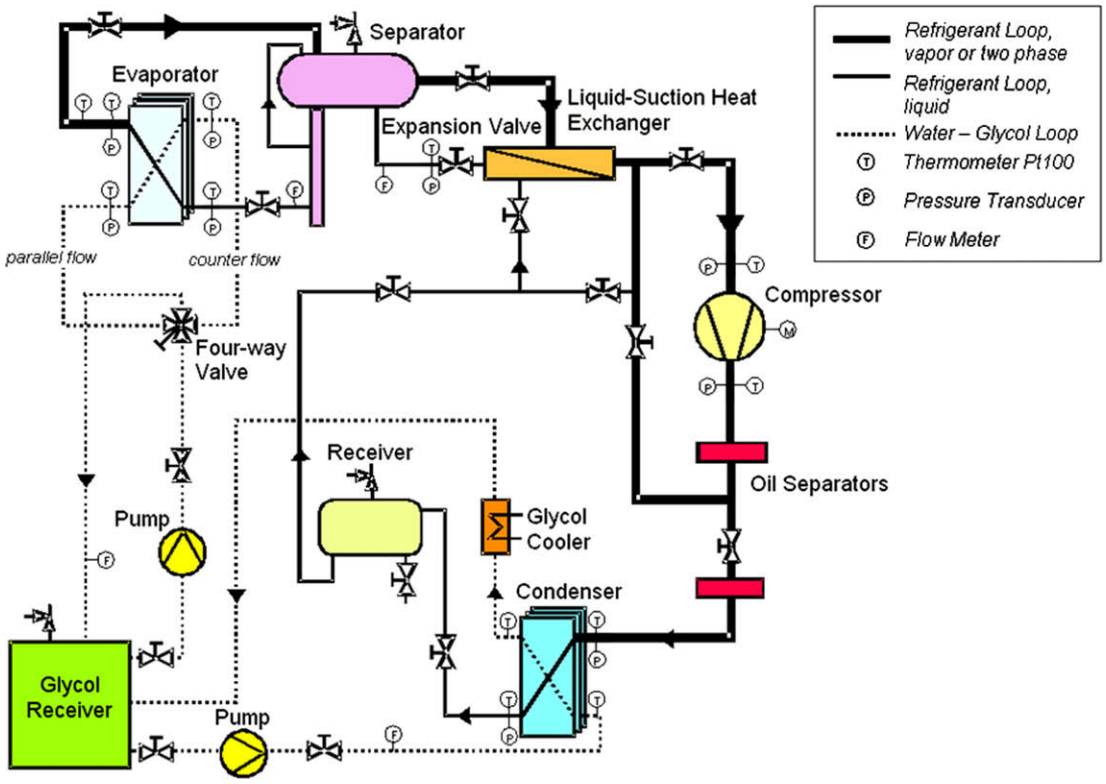

Fig. 1. Experimental setup of the refrigeration compression cycle. Solid lines give the flow of the refrigerant, dashed lines the flow of the secondary fluid, a water/ethylene glycol mixture.

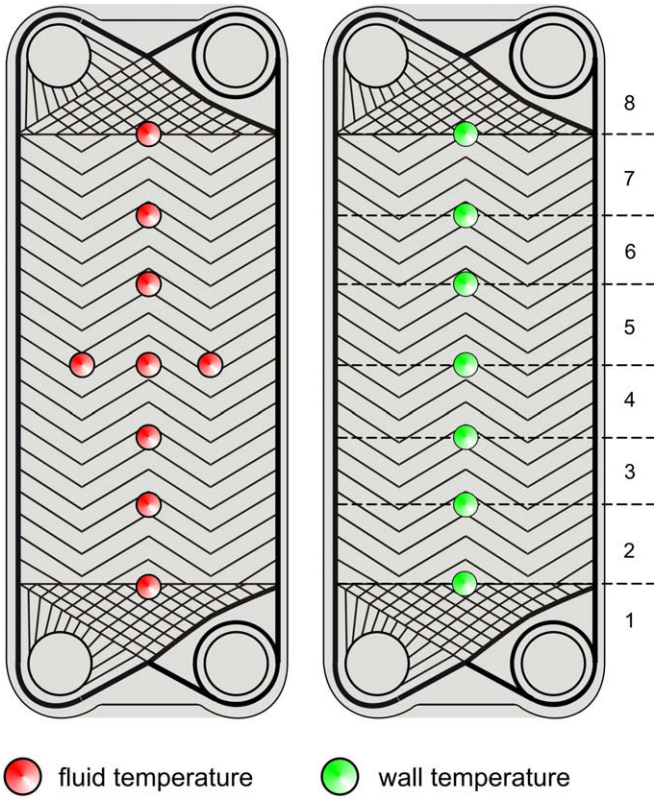

Fig. 2. Position of the thermocouples along one plate to measure the temperature of the heating fluid and the plate wall surface.

small dimples of silver solder to have a smooth surface and optimum thermal contact. The fluid temperature thermocouples are fixed by soldering the wire a few millimeters below the temperature sensitive head in a corrugation valley and bending the thermocouple head up into the middle of the fluid flow channel. A calibration procedure with single-phase flow on both sides of the PHE was necessary repeatedly to ensure that these thermocouples give reliable temperature readings within 0.1 K.

Table 1
Geometrical data of the chevron plates

Length L_{pl} (mm)	872
Width B_{pl} (mm)	486
Amplitude a (mm)	1.6
Wave length Λ (mm)	12
Plate thickness δ_{pl} (mm)	0.6
Thermal conductivity λ_{pl} of the plates (W/mK)	15
Chevron angle (°) type A	63
Chevron angle (°) type B	27

The evaporator is operated in a flooded thermosyphon mode as shown in Fig. 3. This liquid-overfeed operation, although mechanically pumped rather than gravity driven as in our case, is common in industrial refrigeration and chillers. The advantage of the flooded operation mode is that the entrance condition for the refrigerant into the evaporator is well defined, much better than in the direct expansion mode. An expansion valve for the refrigerant in front of the evaporator leads to partial evaporation (flash) in the entrance region and maldistribution of refrigerant between the plates, as described by Vist and Pettersen [11]. The evaporator entrance vapor qualities for direct expansion typically vary between 0.1 and 0.2. A second drawback of the direct expansion mode is the transition from boiling two-phase heat transfer to single-phase heat transfer (dryout) of the superheated vapor somewhere inside the PHE. This transition gives an additional uncertainty on behalf of the area inside the PHE in which evaporation takes place and which can only be accessed by an energy balance equation. These drawbacks are avoided in the flooded operation mode, where the entrance

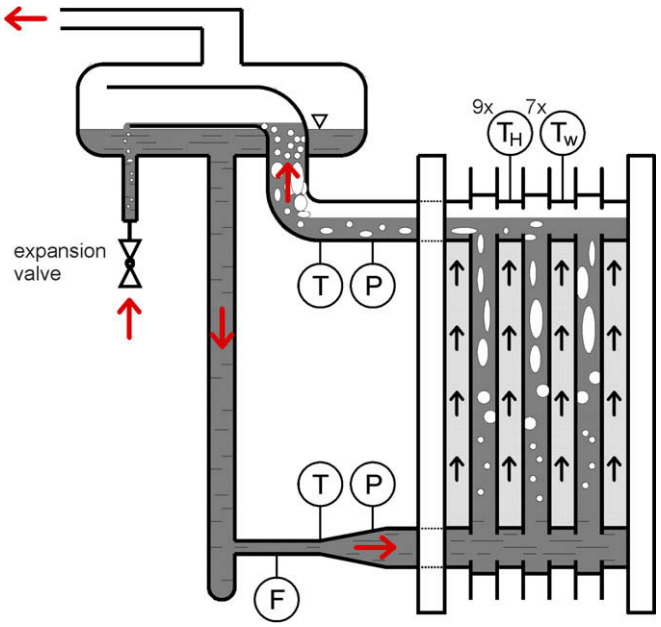

Fig. 3. The evaporator setup operating in a flooded thermosyphon mode. The heating fluid can be in parallel flow (shown here) or in counter flow. *T* indicates temperature measurement locations, *p* shows pressure measurement locations, and *F* indicates a flow rate measurement.

condition of the refrigerant can be adjusted to be liquid with a very small and well-known subcooling and the superheating of the refrigerant vapor is delayed into the liquid-suction heat exchanger. The vapor quality $\dot{x}$ at the exit of the evaporator can be calculated by means of an energy balance equation, it depends on the operating conditions and varies between $0.5 < \dot{x} < 0.9$ in our experiments.

Because of the thermosyphon operation mode, the refrigerant mass flux in the evaporator is typically greater than the mass flux within the loop, so two flow meters are needed on the refrigerant side, see Fig. 1. A turbine flowmeter and a coriolis flow meter were used. Sight glasses allow for a check on the amount of bubbles in the liquid refrigerant, which must be low to give reliable readings. The Krohne turbine flowmeter was calibrated to ammonia and R134a and gives an uncertainty of less than 2%, while the Micro-motion coriolis type flowmeter was calibrated inhouse to an uncertainty of less than 1.5%. Temperatures at the inlet and outlet ports of all heat exchangers are taken with Pt100 resistant thermometers calibrated against a PTB standard (Physikalisch Technische Bundesanstalt Braunschweig, Germany), differential and absolute pressures are measured with Holox-membrane pressure transducers. The heating fluid is a mixture of 35% ethylene glycol and water. The heating fluid for the evaporator is directed either in parallel flow or counter flow by switching a 4-way valve shown in the overall setup, Fig. 1. The flow rate of the heating fluid through the evaporator is adjusted by a speed controlled pump, the temperature of this heating fluid is adjusted by an extra heat exchanger with external cooling water.

In the refrigeration system a 55 kW 6-cylinder BOCK F16 compressor is used, which allows working with either 2, 4 or all 6 cylinders, thus achieving different volume flow rates in the refrigerant loop. Two oil separators in a row are applied to keep the oil content as low as possible. Refrigerant samples taken from the outlet of the condenser showed that the oil content in the evaporator and condenser never reached more than 0.2% in weight. The expansion valve in our setup was operated manually to allow for a specific setting and adjustment of the operation condition. All temperature, pressure and flow rate data was handled by a LABVIEW data acquisition system which allowed for instant energy balance checks while operating the setup. More details of the experimental setup can be found in [13].

3. Data reduction

In this section the calculation of the quasi-local evaporation heat transfer coefficients along a plate from the thermocouple readings, the mass fluxes and the refrigerant pressure readings is outlined. The thermocouples within one heating fluid plate channel allow the definition of eight control volumes along one plate as shown in Fig. 2. In the middle of the plate three fluid thermocouples are placed horizontally next to each other to check on a maldistribution within one channel. These thermocouples always showed equal temperatures within ±0.15 K, thus lateral flow maldistribution over a plate channel seems negligible. Extra thermocouples at the inlet and the exit of each heating fluid plate channel (five altogether) were used to check on a possible maldistribution between the plates of the PHE. They indicate that the secondary fluid flow is evenly distributed, while the refrigerant flow in the first and the last plate channel is ca. 10% higher due to adiabatic wall effects of the frame on the heating fluid side. Because of the adiabatic wall, almost two times more heating fluid heat capacity is available for the refrigerant in the outer channels than for the others, causing more refrigerant evaporation there. Typical temperature readings for the fluid and the wall thermocouples are shown in Fig. 4 for a parallel flow situation with R134a at $T_R^s = -7.5\ ^\circ C$ ($p_R^s = 2.2$ bar). The solid lines in Fig. 4 show the measured temperatures of the heating fluid and of the adjacent wall. The dashed lines are calculated temperatures of the plate surface temperature on the refrigerant side and the refrigerant temperature along the plate channel.

The control volumes defined by the thermocouples are of equal size except for the entrance area at the bottom and the exit area at the top of the plate. The heat flux from the heating fluid within the control volume *i* is calculated by

$$\dot{q}_{H,i} = \dot{M}_H \cdot c_{p,H}(T) \cdot [T_{H,i-1} - T_{H,i}]/(2 \cdot A_i), \quad (1)$$

where $\dot{M}_H$ is the mass flow of the heating fluid in one channel and $c_{p,H}$ is the specific heat capacity of this aqueous mixture. A_i is the heat transferring area for one side of this control volume. The local single-phase heat transfer coefficients on the heating fluid side can now be calculated by

$$h_{H,i} = \frac{\dot{q}_{H,i}}{(T_{H,\bar{i}} - T_{w,H,\bar{i}})}, \quad (2)$$

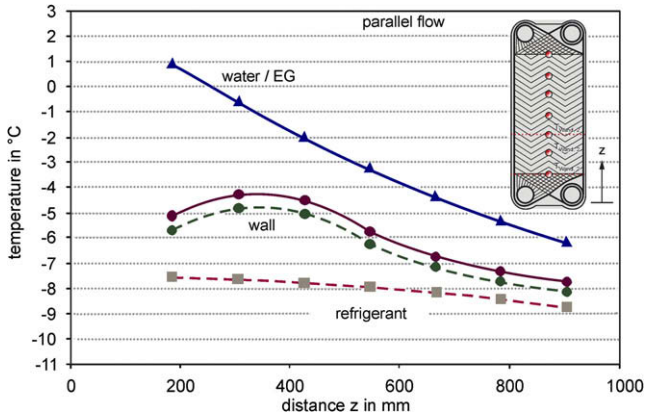

Fig. 4. Typical temperature distribution in a refrigerant and in heating fluid plate channel. A parallel flow situation with R134a is shown, the dashed line temperature distribution has been calculated.

where $\bar{i}$ indicates mean fluid and the mean wall temperature of this segment, both of which are measured. The single-phase heat transfer coefficients had values ranging from $h_H = 2080\ W/m^2\ K$ ($Nu_H = 31.5$) at $\dot{m}_H = 87\ kg/m^2\ s$ ($Re_H = 149$) to $h_H = 6600\ W/m^2\ K$ ($Nu_H = 94$) at $\dot{m}_H = 546\ kg/m^2\ s$ ($Re_H = 1127$). The Reynolds number Re_H and the Nusselt number Nu_H are defined as

$$Re_H = \frac{\dot{m} \cdot d_h}{\eta} \quad \text{and} \quad Nu_H = \frac{h \cdot d_h}{\lambda}.$$

The hydraulic diameter is calculated as $d_h = 4 \cdot a$. Our results for the single-phase heat transfer coefficient compare well with Martin's correlation [14], which is shown in Fig. 5. Fig. 5a gives the experimental single-phase heat transfer coefficient as a function of the mass flux within the plate channel, Fig. 5b gives the same data in dimensionless numbers. To get the heat transfer coefficients on the refrigerant side, the wall surface temperatures on the refrigerant side have to be calculated from the wall temperatures measured on the heating fluid side via one-dimensional heat conduction across the plate:

$$T_{w,R,i} = T_{w,H,i} - \frac{\dot{q}_{H,i} \cdot \delta_{pl}}{\lambda_{pl}}. \tag{3}$$

Here δ_{pl} is the plate thickness and λ_{pl} is the thermal conductivity of the plate material made of stainless steel, both given in Table 1. The quasi-local heat transfer coefficient of the refrigerant is then calculated by

$$h_{R,i} = \frac{\dot{q}_i}{T_{w,R,i} - T_R^s(p_R)}, \tag{4}$$

where $T_R^s(p_R)$ is the saturation temperature of the refrigerant as a function of the local pressure at this location. To get the heat transfer coefficient $h_{R,i}$ in dependence of the vapor quality instead of the location along the plate, an energy balance equation of the type

$$\Delta\dot{x} = \frac{\dot{q}_i \cdot A_i}{\dot{M}_R \cdot \Delta h_v(T_R^s)} \tag{5}$$

is used for each control volume, $\Delta h_v(T_R^s)$ being the enthalpy of vaporization of the refrigerant. Within the first control volume, the slight subcooling of the refrigerant entering the PHE has to be taken into account on the basis of the temperature difference $T_{R,in} - T_R^s(p_R)$. The subcooling of the refrigerant entering the evaporator in our experiments was always less than 2 K, so saturation temperature was reached within the first control volume.

As the temperature difference in the denominator of Eq. (4) is small, the saturation temperature of the refrigerant has to be calculated with great care. An increase of the saturation temperature of the refrigerant due to the oil content is one possible cause of error; a flawed pressure reading may be another. As the oil is a component with a high boiling temperature, even small amounts of oil dissolved into the refrigerant will influence the saturation boiling curve of the refrigerant/oil mixture significantly. Fortunately, the dew line is much more affected than the bubble line for small oil contents. Since the oil content is kept very low, the saturation temperature of the pure refrigerant is used.

The overall pressure loss measured between the refrigerant inlet and outlet consists of the pressure drop of the ports and manifolds, as well as the head pressure due to gravity, acceleration and friction. We used the pressure drop model for ports and manifolds by Shah and Focke [15] and the heterogeneous pressure drop model based on the Lockhard–Martinelli approach for the frictional part as described in [16]. The pressure drop of the refrigerant R134a in this natural thermosyphon loop ranged between $\Delta p = 0.105$ bar ($\dot{m}_R = 30\ kg/m^2\ s$; $p_R^s = 2.5$ bar) and $\Delta p = 0.112$ bar for $\dot{m}_R = 77.5\ kg/m^2\ s$ at $p_R^s = 4.1$ bar. The calculated pressure drop matched the measured value with less than 10% deviation in all experiments.

The uncertainty analysis takes into account the uncertainties of the thermophysical properties propagating into the heat transfer coefficient as well as the uncertainties of the measurement devices. Details are given in [13]; uncertainties of the major instruments have been pointed out in Section 2. The result of the uncertainty analysis is exemplified in Fig. 6 where the measurement results of the quasi-local heat transfer coefficient for ammonia at $p_s = 5.5$ bar ($T_R^s = 280$ K) in a plate of type A in a parallel flow flooded evaporator is shown with the resulting error bars. The

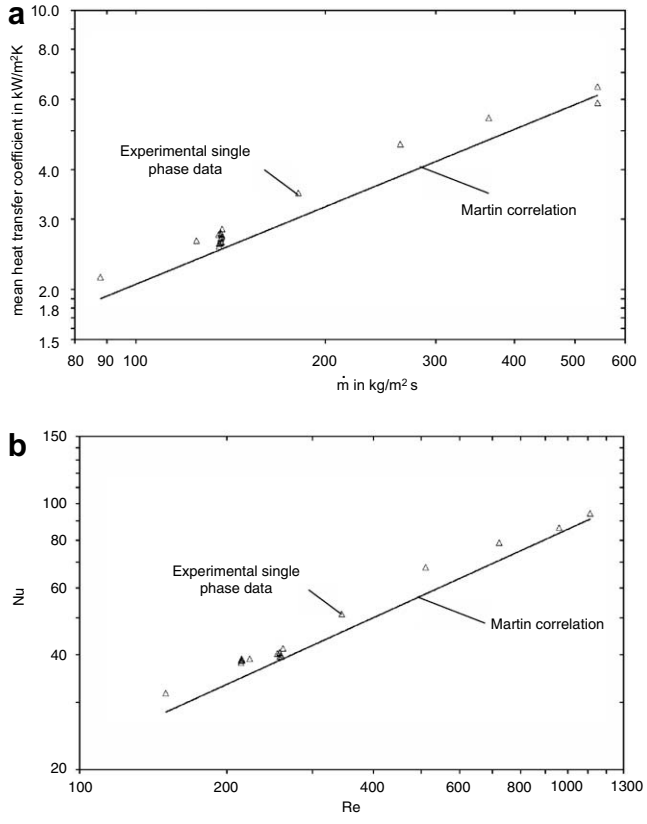

Fig. 5. (a) Experimental single-phase heat transfer coefficients on the heating fluid side (water/ethylene glycol) as a function of mass flux, compared with Martin's correlation [14]. (b) The experimental Nusselt number for the single-phase heat transfer as a function of the Reynolds number.

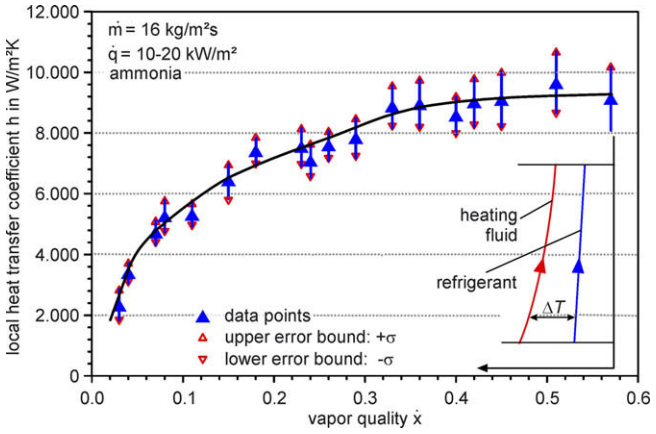

Fig. 6. Error bars resulting from an uncertainty analysis for a typical parallel-flow situation with ammonia in plates of type A.

uncertainty for the experimental value of the refrigerant heat transfer coefficient rises from 6% at low vapor fractions to 15% at high vapor fractions as the temperature between the heating fluid and the refrigerant decreases.

4. Results and discussion

4.1. Results for R134a

Experimental results on local heat transfer coefficients are shown for refrigerant R134a first. In Fig. 7 the quasi-local heat transfer coefficients are given as a function of the local vapor quality. These values are gained from an energy balance for a plate segment of ca. 100 mm length, see the previous section, thus they are called quasi-local values. The plate type used for the data in Fig. 7 has a chevron angle of $\varphi_A = 63°$ (type A), the saturation temperature of the refrigerant is $T_R^s = 268$ K ($p_R^s = 2.42$ bar). At this parallel flow arrangement there is a strong increase in the heat transfer coefficient as the vapor fraction rises to about 0.2. Please note that these local values do not translate into succeeding values along the plate length within one specific run, as the local heat flux changes significantly along the plate. All the data points in this and the following figures have been sorted into groups of similar mass fluxes and similar heat fluxes to be comparable, taking many runs with different temperature differences $(T_H - T_R^s)$ between heating fluid and refrigerant. For smaller heat and mass fluxes the heat transfer coefficient for this plate type seems to decline after running through a maximum at a vapor quality of about $\dot{x} = 0.5$, see also Fig. 10. Unfortunately we were not able to get high vapor qualities for the lower heat flux values in Fig. 7. It is also apparent in Fig. 7 that a rising heat fluxes give a small rise in the heat transfer coefficients only for $\dot{x} > 0.4$. This is contrary to the usual assumption that, for small and medium vapor qualities, the nucleate boiling is dominating. The experimental data on R134a from Yan and Lin [3] is included in Fig. 7, as these can be considered quasi-local values as well. There is a sufficient agreement between their data (using a herringbone plate) for R134a at $T_R^s = 270$ K and ours.

In Figs. 8 and 9, parallel flow and countercurrent flow situations are analysed for refrigerant R134a. The refrigerant flow is always bottom-up, the heating fluid flows either bottom-up (parallel flow) or top-bottom (counter flow). In Fig. 8, an overall *mean* heat transfer coefficient for the plate is shown as a function of the exit vapor quality. The saturation temperature for the mass flux of $\dot{m}_R = 50$–60 kg/m² s shown in Fig. 8 is $T_R^s = 283$ K ($p_R^s = 4.13$ bar); the saturation temperature for the mass flux of $\dot{m}_R = 80$–90 kg/m² s is $T_R^s = 273$ K ($p_R^s = 2.91$ bar). The mean heat transfer coefficient for the refrigerant is calculated by

$$\frac{1}{h_R} = \frac{1}{U} - \frac{1}{h_H} - \frac{\delta_{pl}}{\lambda_{pl}} \tag{6}$$

and the overall heat transfer coefficient U as

$$U = \frac{\dot{Q}}{A \cdot \Delta T_{lm}}. \tag{7}$$

In this equation $\dot{Q}$ is the overall heat flow which the refrigerant receives from one plate, ΔT_{lm} is the logarithmic mean temperature difference between the heating fluid and the refrigerant for countercurrent flow and for parallel flow, respectively. The parallel flow case shows more than 10% higher heat transfer values and higher outlet vapor quality values compared to the counter flow arrangement under similar operation conditions. These results are further analyzed in Fig. 9, which shows the vapor quality as a function of the plate position for two similar parallel flow cases and corresponding counter flow cases. The mass flux based on the cross section of one plate channel was about 52 kg/m² s in all cases, the saturation temperature was $T_R^s = 283$ K ($p_R^s = 4.13$ bar). The vapor quality rises very fast in the parallel flow case because of the large temperature difference at the entrance. This can also be seen in

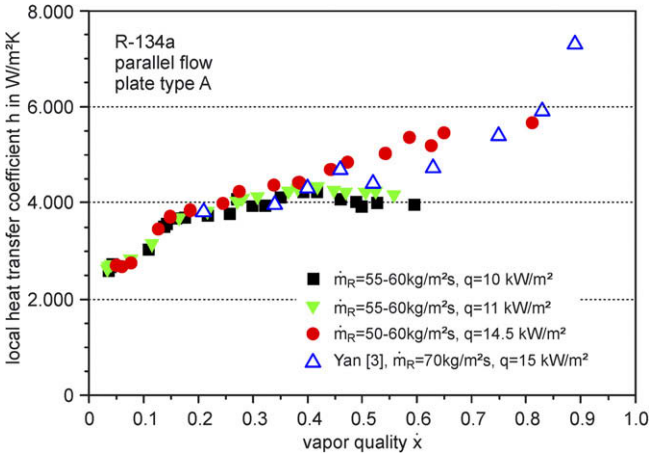

Fig. 7. Results for the quasi-local heat transfer coefficient h as a function of vapor quality $\dot{x}$ for R 134a. Curves for different heat fluxes and literature data from Yan and Lin [3] are shown.

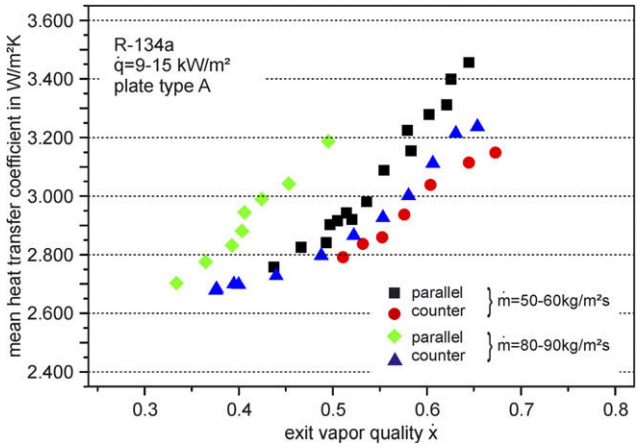

Fig. 8. Plate average *mean* heat transfer coefficients for R134a as a function of *exit* vapor quality. Two different mass fluxes are shown for parallel and counter flow situation each.

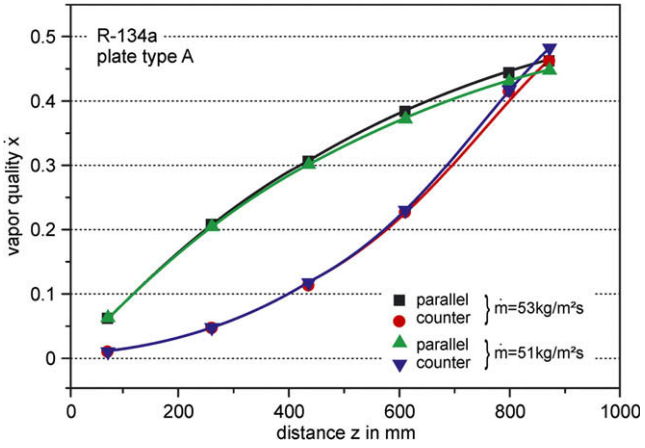

Fig. 9. Evolution of the local vapor quality along the plate. The parallel flow situation is compared to the counter flow.

Fig. 4, where the temperatures are plotted as a function of the plate length, measured from the inlet port upwards. The vapor quality at the exit of the first control volume is $\dot{x}_{\text{parallel}} = 0.2$ compared to $\dot{x}_{\text{counter}} = 0.08$ in the countercurrent flow case.

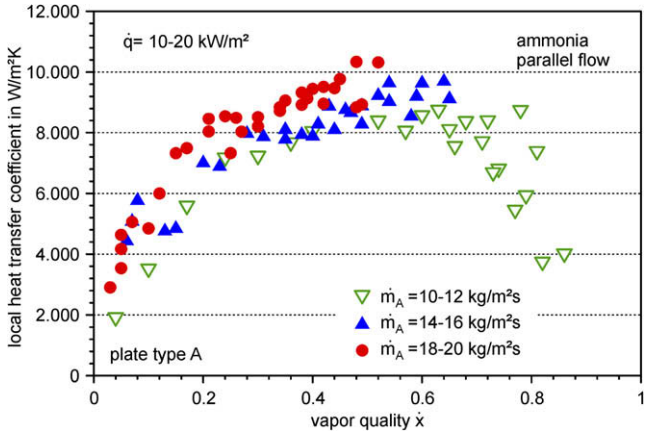

Fig. 10. Results for the quasi-local heat transfer coefficient h as a function of vapor quality $\dot{x}$ for ammonia. Different mass fluxes are shown.

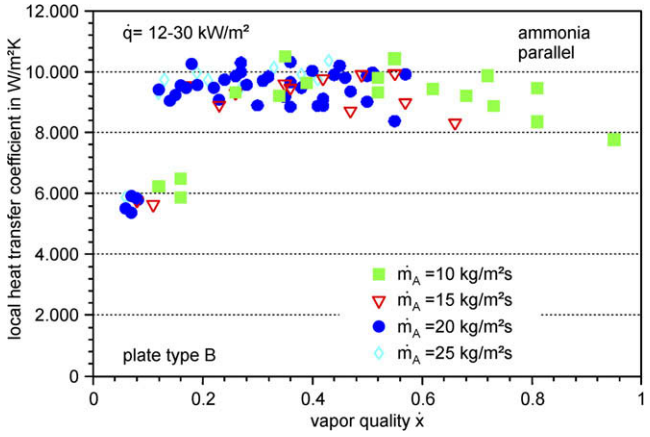

Fig. 11. Quasi-local heat transfer coefficient h as a function of vapor quality x of ammonia. in a low chevron angle plate of type B. Different mass fluxes are shown.

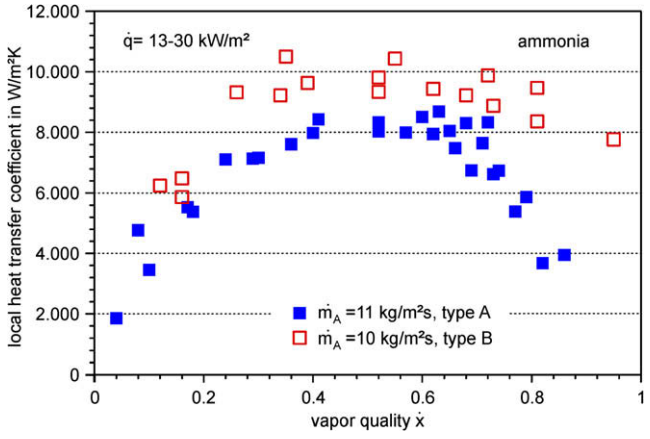

Fig. 12. Comparison of local evaporation heat transfer coefficients of ammonia for two different plate types A and B. Plate A has a high chevron angle of $\varphi_A = 63°$, plate B a low chevron angle of $\varphi_B = 27°$.

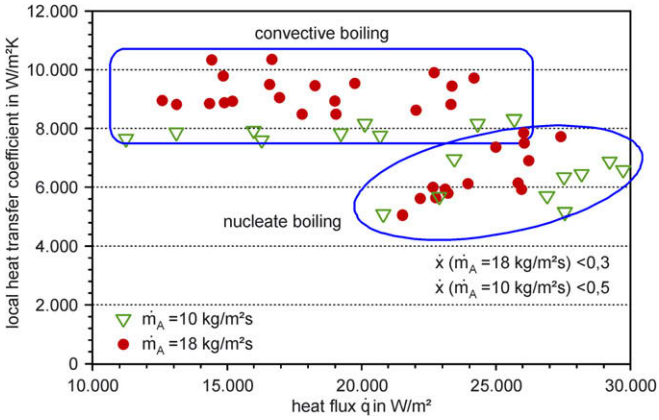

Fig. 13. Quasi-local heat transfer coefficients for ammonia shown as a function of heat flux $\dot{q}$. Two different mass fluxes are shown. Both convective and nucleate boiling mechanisms can be identified.

4.2. Results for ammonia

In Figs. 10–13 results for ammonia as the refrigerant fluid are shown. Fig. 10 shows data for a heat flux situation similar to the R134a case in Fig. 7, but the mass flux is different. This data has been gained at an ammonia saturation temperature of $T_R^s = 283$ K ($p_R^s = 6.12$ bar) at the low mass flux of 10 kg/m^2 s and a saturation temperature of $T_R^s = 270$ K ($p_R^s = 3.81$ bar) at the high mass flux of 20 kg/m^2 s. These results for plate type A show a similar behavior in dependence of the vapor quality as for R134a, except that the ammonia heat transfer values are almost twice as high as for the HFC refrigerant, even though the mass flux is lower. This well known result is mostly due to the favorable liquid thermal conductivity λ of ammonia, which is $\lambda_{NH3} = 0.54$ W/m K as compared to $\lambda_{R134a} = 0.098$ W/m K for R134a, each at the temperature of 270 K. Again the heat transfer coefficient in Fig. 10 drops down for low mass fluxes and high vapor qualities. Unfortunately there is not enough data for R134a to check if this would occur for R134a as well.

Quasi-local heat transfer coefficients for the low chevron angle plate B are shown in Fig. 11. This data holds true for an ammonia saturation temperature of $T_R^s = 283$ K ($p_R^s = 6.12$ bar) at the low mass flux of 10 kg/m^2 s and a saturation temperature of $T_R^s = 268$ K ($p_R^s = 3.53$ bar) at the high mass flux of 25 kg/m^2 s. Again there is a strong rise for low vapor quality values, but only a minor decline at high vapor qualities. A direct comparison between plates of type A and B is made in Fig. 12. Both curves show a parallel flow situation with comparable heat and mass fluxes at a saturation temperature of $T_R^s = 283$ K. An important result from Fig. 12 is that low chevron angles are favorable for evaporation in PHEs. The decline in heat transfer coefficients for higher values of vapor quality shows that, different to single-phase heat transfer in PHEs, the strong deflections are not effective and may lead to partial dryout. Fig. 13 shows the quasi-local heat transfer coefficient as a function of the heat flux $\dot{q}$ at saturation temperature of $T_R^s = 283$ K for the lower mass flux and of $T_R^s = 273$ K at the higher mass flux of $\dot{m}_R = 18$ kg/m^2 s. This diagram shows that the nucleate boiling and the convective boiling regimes can be identified to some extend in evaporation within PHEs. More data is needed to clarify the limits and the overlap of these two mechanisms.

In Fig. 14 a comparison of the experimental data already introduced in Fig. 10 with the Steiner–Taborek correlation and the Danilova correlation is made. While the version of the Steiner equation that we used is fitted to vertical tube situations [1], the Danilova equation is directly derived from their work on PHEs. The Steiner correlation has to be supplied with two single-phase heat transfer coefficients, assuming the mass flow is all liquid

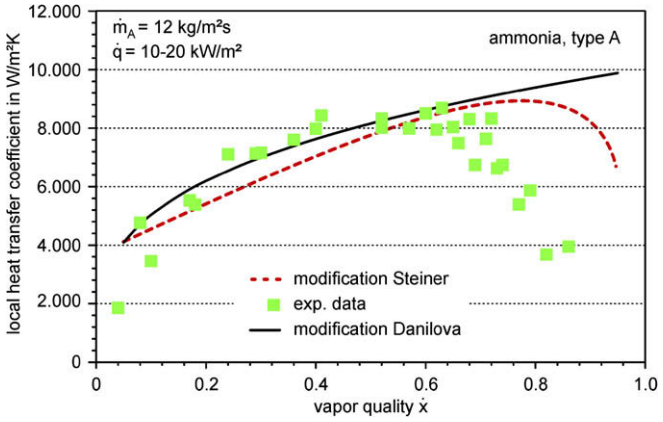

Fig. 14. Comparison between experimental heat transfer data for ammonia in plate type A and two empirical correlations. The Steiner equation for vertical tubes [1] has been scaled down by a factor of 0.51 to match the experimental data points, the Danilova correlation was scaled up by a factor of 1.15 as compared to its original version [2].

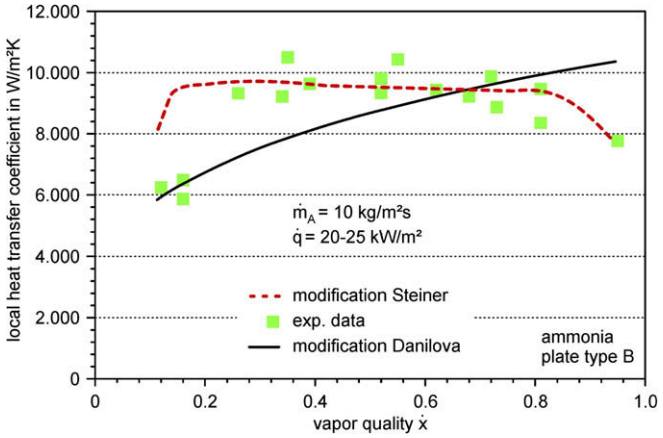

Fig. 15. Comparison between experimental heat transfer data and two correlations for ammonia in plate type B. In this case the original Steiner equation for vertical tubes [1] has been scaled down by a factor of 0.82, the Danilova correlation [2] has been scaled up by a factor of 1.36.

and all vapor, respectively. We used Martin's correlation [14] for the single-phase flow in PHEs for these coefficients. The Steiner correlation overpredicts the data for the type A plate by a factor of two, which indicates that the evaporation in vertical tubes may be superior to the evaporation in PHEs for the situation having high chevron angles of $\varphi = 63°$ considered here. Of course this is only one aspect of the overall performance of a PHE, this drawback may well be compensated for by a more effective heat transfer on the heating fluid side (see Fig. 15).

The Danilova correlation, which reads

$$h_{DAN} = 4.2 \cdot Re_G^{0.3} \cdot Bo^{0.33} \cdot Re_s^{0.2} \cdot \frac{\lambda_l}{d_n} \tag{8}$$

with

$$Re_G = \frac{w_G \cdot d_h}{v_G} \quad w_G = \frac{\dot{x} \cdot \dot{m}}{\rho_G} \quad Re_S = \frac{\dot{q} \cdot d_h}{\Delta h_v \cdot \eta_l}$$

and the Bond number $Bo = \frac{g \cdot \rho_l \cdot d_h^2}{\sigma}$ performs quite well for all our data except for the decline in heat transfer coefficients at high vapor qualities for the type A plates. The index l indicates the liquid phase at saturation conditions, the characteristic length in the Bond number and the Reynolds number is the hydraulic diameter $d_h = 4 \cdot a$. Please note that this definition of the hydraulic diameter differs from the definition of d_h^* used in the single phase heat transfer correlation by Martin [14] as described above.

5. Summary

This paper reports on experimental data of the quasi-local heat transfer during evaporation of ammonia and R134a in PHEs. The saturation temperature varied between 268 K $< T^s_{NH3} <$ 283 K (3.55 bar $< p^s_R <$ 5.73 bar) for ammonia and 265 K $< T^s_{R134a} <$ 283 K (2.157 bar $< p^s_R <$ 4.14 bar) for R134a. The heat transfer coefficient is strongly correlated with the vapor quality. The heat transfer coefficient rises for high values of mass flux but decreases for low mass fluxes after a maximum value at vapor qualities about $\dot{x} \simeq 0.5$. Evaporation heat transfer is, as expected, significantly higher for ammonia than for R134a. Both mass and heat flux raise the heat transfer coefficient to some extend, indicating that both convective and nucleate boiling mechanisms are present. The low chevron angle of the type B plate is beneficial for evaporation. Parallel flow arrangement gives higher effectiveness compared to countercurrent flow. The Steiner boiling correlation for vertical tubes can be adapted to plate evaporators, but more data is needed to modify this equation into a valid predictor of PHE evaporator performance.

Acknowledgements

The research visit of the first author in Hamburg was financed by the German Academic Exchange Bureau DAAD. The setup was supported in part by GEA Ecoflex GmbH, Sarstedt, Germany.

References

[1] D. Steiner, J. Taborek, Flow boiling heat transfer in vertical tubes correlated by an asymptotic model, Heat Transfer Eng. 13 (1992) 43–69;
see also: D. Steiner, Stroemungssieden gesaettigter Fluessigkeiten, in: VDI-Waermeatlas, 10th ed., Springer, Berlin, 2006 (Chapter Hbb).
[2] D.N. Danilova et al., Heat transfer in different plate geometries, Kholod. Tek. 4 (1981) 25–31;
see also: R. Osterberger, B. Slipcevic, Waermeuebergang beim Blasensieden in Plattenverdampfern (Heat Transfer at Nucleate Boiling in Plate Heat Exchangers), Ki Klima-Kälte-Heizung 11 (1990) 481–483.
[3] Y.Y. Yan, T.F. Lin, Evaporation heat transfer and pressure drop of refrigerant R134a in a plate heat exchanger, ASME J. Heat Transfer 121 (1999) 118–127.
[4] Y. Hsieh, T.P. Lin, Saturated flow boiling heat transfer and pressure drop of refrigerant R410A in a vertical plate heat exchanger, Int. J. Heat Mass Transfer 125 (2003) 852–857.
[5] S. Wellsandt, Heat transfer and pressure drop in a plate type evaporator, Ph.D. Thesis, Department of Heat and Power Technology at Chalmers University of Technology, Gothenburg, Sweden, 2001.
[6] G. Longo, A. Gasparella, Experimental heat transfer coefficients and pressure drop during refrigerant R134a vaporization inside a commercial brazed plate heat exchanger, in: Proceedings of the IIR Conference, Vicenza, Italy, 2005.
[7] G. Longo, A. Gasparella, R. Sartori, Experimental heat transfer coefficients during refrigerant vaporisation and condensation inside herringbone-type plate heat exchangers with enhanced surfaces, Int. J. Heat Mass Transfer 47 (2004) 4125–4136.
[8] D. Sterner, B. Sunden, Performance of plate heat exchangers for evaporation of ammonia, Heat Transfer Eng. 27 (2006) 45–55.
[9] D.-H. Han, K.-J. Lee, Y.-H. Kim, Experiments on the characteristics of evaporation of R410A in brazed plate heat exchangers with different geometric configurations, Appl. Therm. Eng. 23 (10) (2003) 1209–1225.
[10] B. Thonon, A. Feldman, L. Margat, C. Marvillet, Transition from nucleate boiling to convective boiling in compact heat exchangers, Int. J. Refrigerat. 20 (8) (1997) 592–597.
[11] S. Vist, J. Pettersen, Two-phase flow distribution in compact heat exchanger manifolds, Exp. Therm. Fluid Sci. 28 (2004) 209–215.
[12] B. Watel, Review of saturated flow boiling in small passages of compact heat exchangers, Int. J. Therm. Sci. 42 (2003) 107–140.
[13] M. André, Waermeuebergang bei der Verdampfung von Ammoniak in Plattenwaerme- uebertragern (Heat transfer during evaporation of ammonia in plate heat exchangers), Ph.D. Thesis, Institute of Thermodynamics, University of Hannover, Germany, 2004.
[14] H. Martin, A theoretical approach to predict the performance of chevron-type plate heat exchangers, Chem. Eng. Process. 35 (1996) 301–310.
[15] R.K. Shah, W. Focke, Plate heat exchangers and their design theory, in: Heat Transfer Equipment Design, Hemisphere Publ. Corp., New York, 1988.
[16] H.-D. Baehr, K. Stephan, Heat and Mass Transfer, Springer Corp., Berlin, 1998.